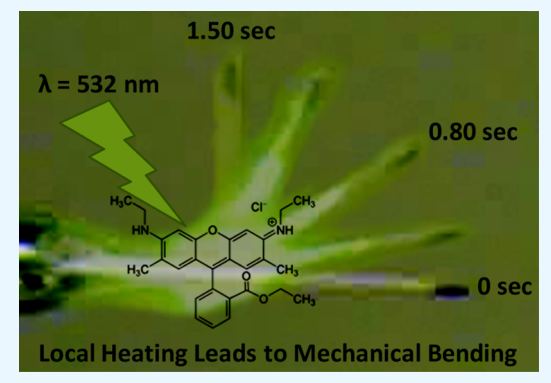


# Generating Photonastic Work from Irradiated Dyes in Electrospun **Nanofibrous Polymer Mats**

Maksim Y. Livshits, †,§ Anton O. Razgoniaev, \*Roberto C. Arbulu, Jisoo Shin, Brad J. McCullough, Yang Qin, <sup>†</sup> Alexis D. Ostrowski, \*, <sup>‡</sup> and Jeffrey J. Rack \*, <sup>†</sup>, <sup>§</sup>

Supporting Information

ABSTRACT: For solar-driven macroscopic motions, we assert that there is a local heating that facilitates large-scale deformations in anisotropic morphologic materials caused by thermal gradients. This report specifically identifies the fate of heat generation in photonastic materials and demonstrates how heat can perform work following excitation of a nonisomerizing dye. Utilizing the electrospinning technique, we have created a series of anisotropic nanofibrous polymer mats that comprise nonisomerizing dyes. Polymers are chosen because of their relative glass transition temperatures, elastic moduli, and melting temperatures. Light irradiation of these polymer mats with an excitation wavelength matching the absorption characteristics of the dye leads to macroscopic deformation of the mat. Analysis of still images extracted from digital videos provides plots of angular displacement vs power. The data were analyzed in terms of a photothermal model. Analyses of scanning electron microscopy



micrographs for all samples are consistent to local melting in low  $T_{\rm g}$  polymers and softening in high  $T_{\rm g}$  polymers. Dynamic mechanical analysis allowed for quantification of the modulus change under a given light fluence. We employ these data to calculate a energy conversion efficiency. These efficiencies for the polymer mats are compared to other nonmuscular systems, including a few natural, biological samples.

KEYWORDS: photonastic, photobending, photothermal, thermal gradients, bilayer cantilever

#### INTRODUCTION

Macroscale motion is a fundamental property of all living systems and helps to determine their survival in local environments. In plants, nonmuscular macroscale motion is used in many ways from optimizing sun exposure for photosynthetic endeavors to opening and closing petals to guard the ovule.1 Plants motions are classified as either photonastic or phototropic. Photonastic motion is regular, repeatable macroscale movement in a preprogrammed direction.<sup>2</sup> In contrast, phototropic movements are irreversible single occurrence events.3 In all cases of macroscale plant motion, a thermal or photochemical stimulus is applied that triggers a series of biological reactions ending in the plant adjusting and monitoring turgor (rigidity from osmotic pressure) in cells to generate stress, thus enabling shape change.<sup>4-6</sup> There are few organisms that utilize light as a means of propulsion, translocation, or displacement (phototaxis) because on a small scale these detectors are unable to distinguish a single light vector. These detectors are all based on rhodopsin.

Nonmuscular macroscale motion, which mimics biological functionality, is of current interest in the material science and biomedical communities for the development of smart, mechanically adaptable materials that can be stimulated by light.<sup>8–11</sup> Light-induced macroscale bending has been observed in a number of different molecule-based materials consisting of azo containing liquid crystal elastomers, <sup>12-14</sup> single and cocrystals of photochromic compounds, <sup>15-22</sup> and the growing family of photosalient compounds. <sup>23-25</sup> These examples explicitly highlight the importance of molecular isomerization or photochemistry as a critical design element in the generation of macroscopic shape change or stress of the material. Bending requires an elastic gradient, often associated to a concentration gradient, through the material thus establishing a bimorph or bilayer structure. This bilayer structure permits contraction on one side and expansion on the other to permit bending. For example, in shape memory

Received: July 15, 2018 Accepted: October 1, 2018 Published: October 1, 2018



<sup>&</sup>lt;sup>†</sup>Department of Chemistry and Chemical Biology, The University of New Mexico, Albuquerque, New Mexico 87131, United States <sup>‡</sup>Department of Chemistry, Center for Photochemical Sciences, Bowling Green State University, Bowling Green, Ohio 43403, United States

<sup>§</sup>Department of Chemistry and Biochemistry, Ohio University, Athens, Ohio 45701, United States

materials bending is a result of differing thermal properties between two crystalline phases.<sup>26,27</sup> In plants, differential turgor pressure leads to stem bending or twisting.<sup>28</sup> Although molecular motion is important, it is the formation of concentration gradients that actually leads to bending in

For solar-driven macroscopic actuation, we assert that there is necessarily a local heating of the sample that facilitates largescale deformations by accentuating material property differences caused by these anisotropic gradients. Specifically, the origin of the gradient is molecular and photophysical heating. Irradiation of a solid sample results in approximately 4% reflection due to differences in the refractive index between air and the solid sample, as predicted by Snell's law. Light that penetrates the sample and triggers a photochemical event dissipates some of this energies as heat through a variety of photophysical processes. Moreover, unless there is quantitative conversion of light energy to work (macroscopic deformation), the absorbed light energy must be lost as heat. 29,30 This heat is generated from excited state relaxation from the initial Franck Condon state(s) and leads to the observed Stokes' shift in emission. In the absence of emission, excited state deactivation is also a source of heat. For photochromic compounds that undergo a change in molecular structure, some of this excited state energies are lost in the form of work to physically move these molecular components. However, as these processes are exothermic (energetically downhill), they release heat. In solution, heat loss is trivial as it is dissipated into solvent vibrational modes. In solid samples, however, heat transfer to air is notoriously inefficient, and thus the heat generated from molecular light excitation is trapped within the material. We show in this manuscript that heat generated from excited state deactivation (following electronic absorption) can have a substantial effect on the mechanical properties of a soft material (polymer) and even do work in the form of macroscopic photonastic motion.

This report specifically addresses the fate of heat generation in photonastic materials and demonstrates how heat can perform work following excitation of a nonisomerizing dye. We previously published results illustrating light-induced macroscopic bending in a co-polymer of norbornene that was ascribed to isomerization of a pendant photochromic ruthenium sulfoxide unit. $^{31-33}$  We noticed a nontrivial role for photothermal bending in that study. Since then, we have noted literature reports on photosoftening, etc., which appear to imply a significant role for a photothermal or photoinduced heating effect in macroscopic bending of polymer or crystalline materials. 30,34,35 Here, we preform the critical bilayer or bimorph structure for bending by creating nanofibrous mats from electrospinning techniques. The fibers comprise simple dyes that generate heat following visible light excitation from the excited state processes described above. We speculate that the fibers allow for the formation of a thermal and elastic gradient not possible in films. We propose that the heat generated from dye excitation is confined within individual nanofibers, whereas heat distribution from irradiation in films is much more rapid preventing creation bilayer gradients. We quantify the angular displacement of motion of the polymer film as a function of incident power (Q) and relate this to material properties of the polymer. We assign the macroscopic bending of the sample as due to a photothermal effect, where heat is generated from photophysical relaxation processes. In this photothermal regime, one expects the amount of bending

to be dependent upon light exposure, dye concentration, and glass transition and melting temperatures of the polymer, and this is what we observe.

#### ■ METHODOLOGY

Rhodamine 6G was purchased from Sigma-Aldrich and utilized without further purification. Free base tetraphenylporphyrin (H2TPP) was prepared according to previous literature procedures.<sup>36</sup> Poly(lactic acid) (PLA) and poly(caprolactone) (PCL) are both commercially available under the trademarks of Ingeo 4043D (NatureWorks LLC) and InstaMorph (Happy Wire Dog, LLC), respectively. Both polymers are used without any further purification.

Rhodamine 6G- and H2TPP-doped electrospun mats were prepared by adding the dye to polymer (PLA and PCL) in predetermined amounts. 1,2-Dichloroethane is added and left to sit until the polymer is nicely solvated. The solution is spun at ~10 kV over a 12 cm horizontal distance to the collection plate. Once the polymer is spun, it is cut into 10 mm long  $\times$  1 mm wide 0.3-0.5 mm thick pieces. The plain polymer reference mats are prepared under the same conditions without the addition of dye. Rhodamine 6G- and H2TPP-doped dropcast films were prepared by taking a similar solution and pouring the mixture into a mold, which is left exposed to air for slow solvent evaporation. Once dry, the film is removed from the mold and cut into 10 mm long × 1 mm wide 0.5 mm thick pieces. All electrospinning and video recording are conducted on a homemade apparatus, whose description may be found in the Supporting Information. The reflectance, scanning electron microscopy (SEM), and dynamic mechanical analysis (DMA) instrumentation and protocols are also found in the Supporting Information.

#### RESULTS AND DISCUSSION

Shown in Scheme 1 are the dyes and polymers employed in this study. These dyes were chosen because they exhibit

Scheme 1. Structure of Rhodamine 6G (Upper Left), Free Base Tetraphenylporphyrin (Upper Right), Poly(lactic acid) (Bottom Left), and Poly(caprolactone) (Bottom Right) **Employed in This Study** 

moderate to high emission quantum yields.<sup>37</sup> For this study, we required that most of the absorbed light would be lost radiatively through emission and that only a small amount of absorbed photonic energy would be lost nonradiatively as heat. It is important to note that these are simple, commercially

available dyes that do not undergo substantial molecular or electronic structural change upon excitation, unlike photochromic compounds that are often employed for these types of studies.

Polymers are chosen because of their relative glass transition temperatures  $(T_{\rm g})$ , elastic moduli (E), and melting temperatures  $(T_{\rm m})$ . Moreover, it is important that the polymers have a long shelf live as well as stability and suitability for electrospinning. The nanofibrous mats were produced from electrospinning solutions containing a polymer and a dye. In the absence of dye solute, the electrospinning technique generated a relatively uniform fiber distribution (Figure S23) that was laterally aligned from a low-magnification perspective with our instrumentation (Scheme S1). In the presence of dye, the uniform fiber dimension was strongly perturbed, producing relatively large clusters as well as relatively small diameter fibers (Figure 1). On the basis of our experience, we assume

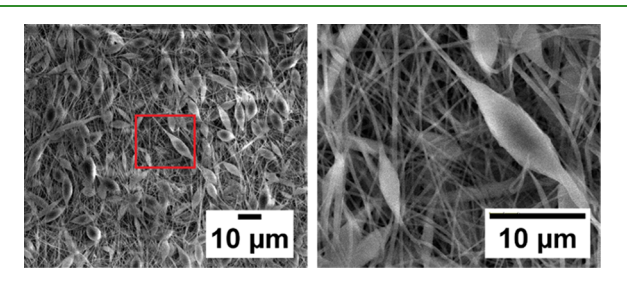


**Figure 1.** SEM micrographs of an unirradiated 0.0025 mM rhodamine PLA electrospun mat at two different magnifications. The red square in the left image is an outline of the higher-resolution right image.

that these structures formed during the electrospinning process and are due to the polymer wrapping or folding itself around the dye during solvent ionization. We want to reiterate that the no clumping is observed in the polymer mats without the dye molecules. Views of smaller areas reveal structural anisotropy in the lateral arrangement as well as in the diameter of the fibers (Figure 1). Indeed, the high surface area and high concentration of fibers do not permit light to transmit through the sample, indicating that all light that impinge upon the sample are either scattered or absorbed.

Light irradiation of the nanofibrous polymer mats with an excitation wavelength (color) matching the absorption characteristics (Figure S1) of the dye leads to macroscopic deformation (bending) of the mat. The nanofibrous mats are typically 10 mm long  $\times$  1 mm wide  $\times$  0.3–0.5 mm thick. Digital videos of the deformation of each representative sample can be found in the Supporting Information. Consistent to a photothermal model where heat is generated following absorption (nonradiative relaxation), the amount of light directed onto the sample and the dye concentration led to different levels of bending. Again, it is important to note that these compounds do not feature a change in a molecular structure following electronic excitation. Normally, much of the incoming light is scattered from the top of the sample resulting in only a small fraction absorbed. Reflectance measurements show that 2-6% of the incident light is absorbed for the samples investigated here (Figure S2).

As described in detail in the Methodology Section, we extracted still images from the digital video utilizing ImageJ (Figure 2).<sup>38</sup> In these videos, the end of the mat was marked with a black dot to enable tracking (Figure 2). Thus, we were able to apply the distance formula to generate a plot of angular position vs time. Shown in Figure 2 are representative data of 0.0025 mM rhodamine 6G in PLA (poly(lactic acid);  $T_g = 60$ °C;  $T_{\rm m}$  = 165 °C; E = ~3400 MPa; 1 mg rhodamine/1 g PLA, 0.001 wt %)<sup>39</sup> irradiated with 75 mW of green light (532 nm). As seen in the videos, deformation of sample is a simple bending of the nanofibrous mat in which the sample forms a 90° angle. Thus, data collection concludes when the sample mat is coincident to the direction of the laser beam. Shown in Figure 3 are a series of these same 0.0025 mM rhodamine 6G in PLA mats irradiated with different incoming powers ranging from 10 to 75 mW. As would be expected, for a photothermal model, greater the light intensity directed onto the sample, led to more rapid deformation. As seen in the 75 and 50 mW traces (Figure 3B), the total time of the experiment (time needed to bend the sample to 90°) was complete within 6 s, where with an intensity of 25 mW directed onto the sample, the time required to bend the sample is greater than 20 s. If too low of light intensity (10 mW) was directed upon the sample, then the sample not only did not bend to 90°, but also the

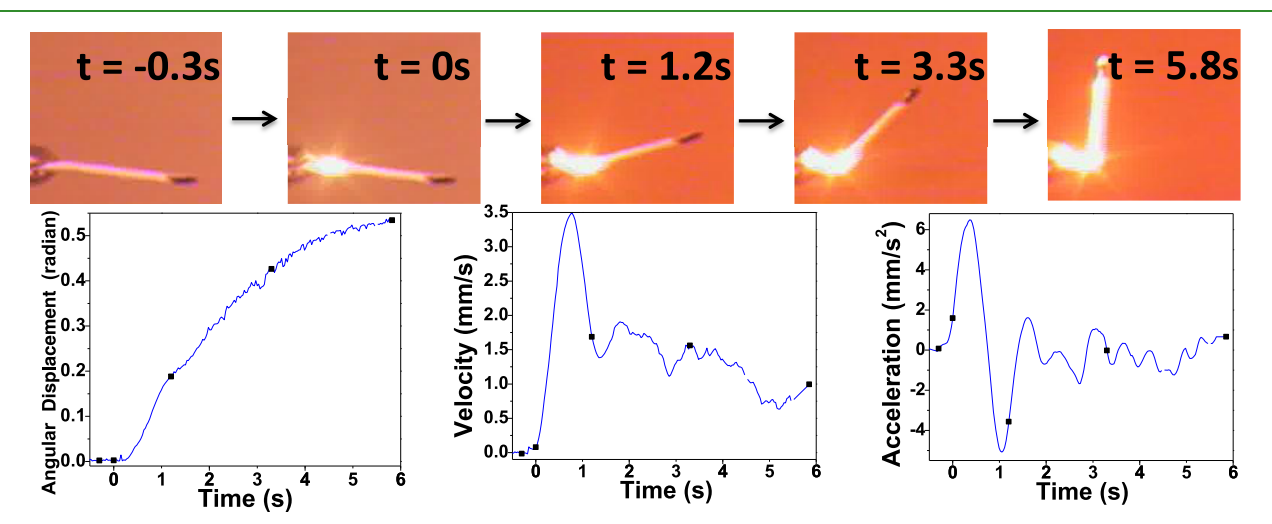


Figure 2. Five still images extracted from the photobending analysis of a 0.0025 mM PLA electrospun polymer mat irradiated with 75 mW, 532 nm light. Below the still images are the calculated angular displacement (left), velocity (middle), and acceleration (right) of the photobending experiment. The five images shown are highlighted with the five black points on each plot for clarity.

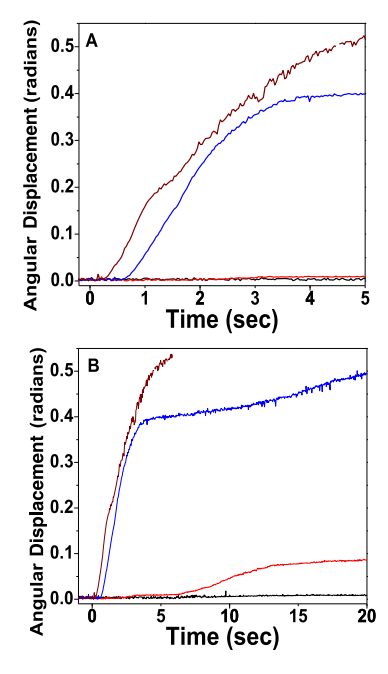


Figure 3. (A) Angular displacement for a 0.0025 mM rhodamine PLA mat irradiated with 10 mW (black), 25 mW (red), 50 mW (blue), and 75 mW (brown) of 532 nm light plotted for the first 5 s. (B) Angular Displacement of the 0.0025 mM rhodamine PLA mat plotted over 20

amount of time to bend the sample was much longer (Figure

This angular displacement with light was investigated with a variety of laser sources. A plot of angular displacement vs power (mW s) for the 75 and 50 mW irradiation samples all show deflection upon exposure to the same amount of total power (~26 mW s) directed onto the sample regardless of the intensity of the laser source (Figure SI4a). The effects of increasing the dye loading in the mats as well as changing the type of dye were explored. We tested samples comprising five different loadings of rhodamine 6G dye (0.0025 mM (0.001 wt %), 0.0048 mM (0.002 wt %), 0.0096 mM (0.004 wt %), 0.0143 mM (0.006 wt %), and 0.0191 mM (0.008 wt %)) and a 0.006 mM (0.002 wt%) H2TPP dye sample in PLA and have observed the same photonastic trend. All angular displacement data as well as subsequent velocity data may be found in the Supporting Information (Figures S3a-e, S4a-b, S5a-e, S9-S11). These observations are consistent to a photothermal mechanism for macroscopic bending of the polymer sample. We note that for a polymer sample containing a larger amount of rhodamine 6G dye (up to 0.0191 mM; 8 mg dye/1 g PLA) that the minimum power and initial energy needed to bend these samples continues to lower, until occurring at ~10 mW s for a 0.0191 mM loading.

A number of control experiments were further performed to confirm the role of the polymer mat anisotropy and activity of the dye. The first control consisted of utilizing a thermoelectric nichrome wire as a heating source at two distances above the polymer mat. Angular displacement generated from the thermal irradiation (Figures S15 and S16) resembled that of the photoirradiated experiment. A second control was to test the role of thermal anisotropy by irradiating a dye-doped film of equal mass to the polymer mat. No angular displacement of the dye film was observed to reinforce the notion that a bilayer or gradient is required to generate stress in a material. It should

also be noted that thermal conductivity has been recently studied though different nanofibers to reveal thermal transport along the through plane backbone of the fiber and not through free space. 40,4

A photothermal macroscopic bending model where heat is supplied from visible light irradiation of dye molecules and transferred to the polymer should display distinct bending patterns depending upon both the melting temperature and glass transition temperature of the polymer. A second common polymer for electrospinning is poly(caprolactone) (PCL;  $T_g =$ -60 °C;  $T_{\rm m} = 58$  °C;  $E = \sim 250$  MPa), which features lower glass transition temperatures and melting temperatures ( $T_{\sigma}$  and  $T_{\rm m}$ ) relative to PLA. When irradiating analogous 0.0025 mM rhodamine 6G in PCL mats under the same conditions as the PLA mats, the angular displacement of the PCL and PLA analogous mats are clearly different, with an unexpected observation that the PCL mats show a slower initial response (Figure 4). Similar to PLA data, the tread that the PCL

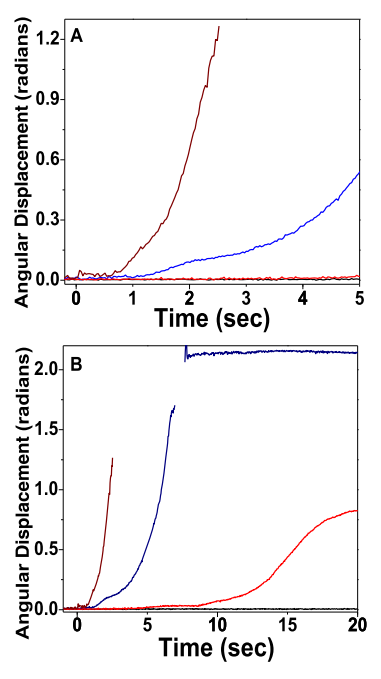


Figure 4. (A) Angular displacement for a 0.0025 mM rhodamine PCL mat irradiated with 50, 75, 100, and 150 mW of 532 nm light plotted for the first 5 s. (B) Angular displacement of the 0.0025 mM rhodamine PCL mat plotted over 20 s.

exhibits a slower to comparable response is valid for the same range of dye loadings as the PLA examples. Data for both the rhodamine and H2TPP for PCL polymer are found in the Supporting Information (Figures S6a-e, S7a,b, S8a-e, S12-S14).

Closer comparison of the SEM micrographs for the 0.0025 mM rhodamine 6G sample in PLA and PCL depicted in Figure 5 reveals an important morphology difference within the irradiation zone. The SEM micrographs of the PCL mats from the lowest to the highest irradiation power mat reveal melting of surface nanofibrous architecture, which is required for the photothermal bilayer bending model proposed here, in contrast to the PLA mats, which show little degradation. In the context of a photothermal bilayer bending model, melting of the 0.0025 mM rhodamine 6G PCL mats at all photoinduced temperatures makes it difficult to establish a **ACS Applied Materials & Interfaces** 

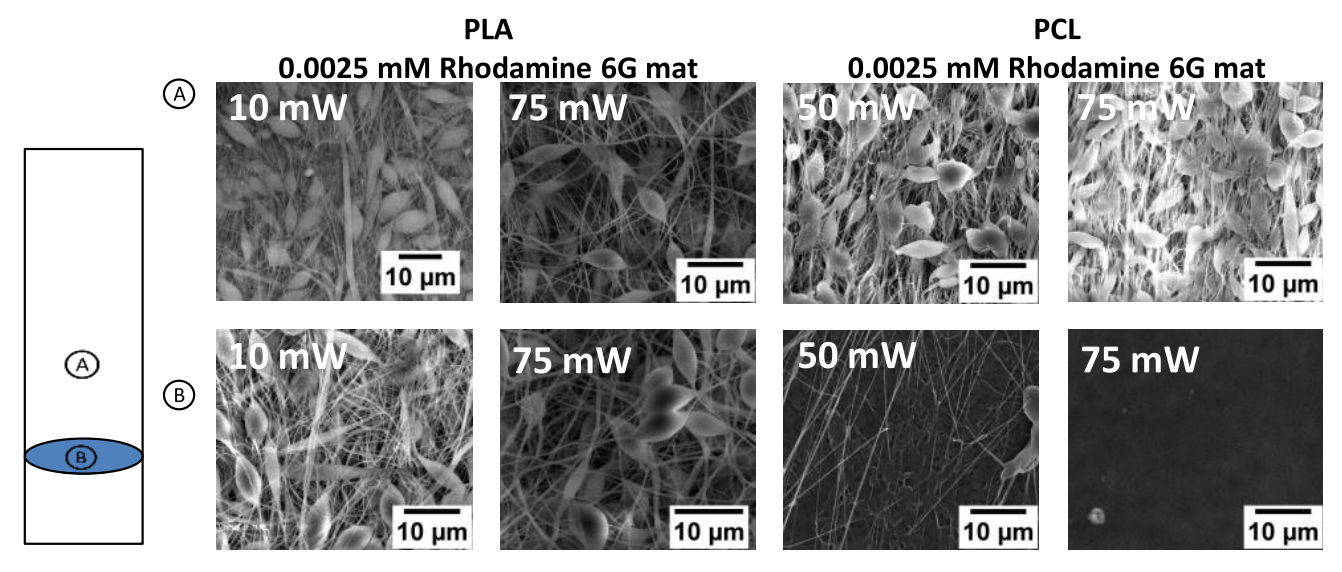


Figure 5. SEM micrographs of analogous 0.0025 mM rhodamine 6G PLA and PCL mats irradiated at two different powers. The left side of the figure is a representation of the polymer mat where the blue area is the irradiation zone. The upper set images are taken from area A, which is outside of the irradiation zone. The lower set of images is taken from area B, which is near the center of the irradiation zone.

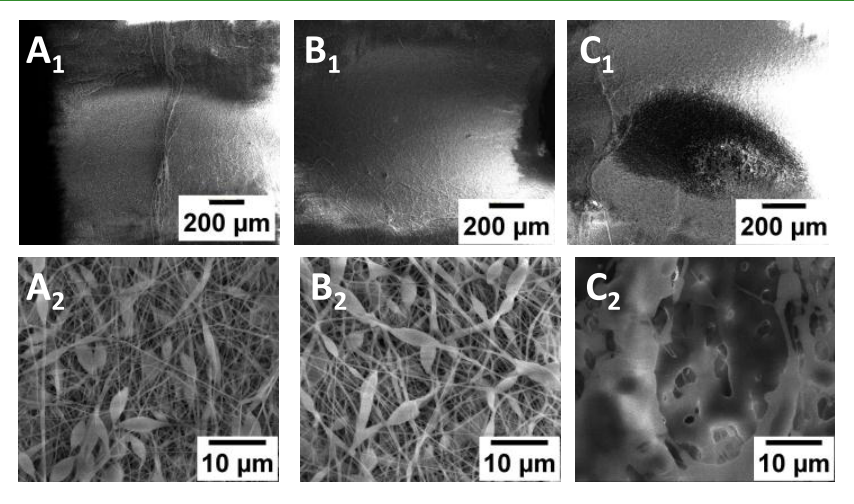


Figure 6. SEM micrographs of the irradiation region for 0.0191 mM rhodamine 6G PLA mats. The micrographs are collected at 200× (first line) and 6500× (second line). Three powers of 10 mW (A), 25 mW (B), and 50 mW (C) are utilized for comparison. Scale bar for (A<sub>1</sub>), (B<sub>1</sub>), and (C<sub>1</sub>) is 500  $\mu$ m and scale bar for (A<sub>2</sub>), (B<sub>2</sub>), and (C<sub>2</sub>) is 20  $\mu$ m.

thermal bilayer in contrast to the PLA mats, which show large tolerance to temperature changes that would set up a thermal gradient. We note that at higher dye loading and higher laser power(s) we observe melting (volume change) of the PLA mats since the radian displacement does not equal 1.57 (90°).

Analysis of the SEM micrographs in Figure 6 reveals a volume change that occurs upon irradiation even when no deformation of the polymer mat is observed. The observation of a contraction in the polymer mat is atypical as a thermal expansion is expected when heating a polymeric material that has been previously observed by Agolini and Gay.<sup>29</sup> Angolini and Gay synthesized a series of azo-aromatic kapton polymers to measure the stress generation while thermally heating and photoirradiating the polymer mats. They report that when thermally heating the kapton film, an initial expansion (10 min) is observed followed by a prolonged (>1 h) contraction of the polymer mat. Irradiation of the kapton mats does not show any expansion. The expansion and contraction are ascribed to thermal expansion and volume change in the trans-cis isomerization, respectively, by the authors even

though the conclusion of the study states that rate of isomerization is not controlling the rate of expansion and contraction. Here, we propose that the observed contraction is due exclusively to a rearrangement of individual polymer strands after a thermal expansion from nonradiative heating.

Linear dynamic mechanical analysis (DMA) was performed on the polymer mats to quantify the changes in complex modulus  $(E^*)$  during irradiation of the polymer mats. The polymer mats were irradiated with 100 mW cm<sup>-2</sup> 532 nm continuous-wave (CW) laser light to observe softening, but avoid melting and irreversible deformation of the mats. Depicted in Figure 7 are the complex modulus changes for 0.0191 mM (8 mg rhodamine 6G/1 g of polymer) rhodamine 6G in PLA and in PCL irradiated with 532 nm light three times.

As expected in a photothermal macroscopic bending model, an immediate softening was observed in the polymer mat upon irradiation of light. Conversely, the polymer mat hardened when the light was removed. A small plastic deformation in the polymer mat was observed in the DMA after the first cycle of

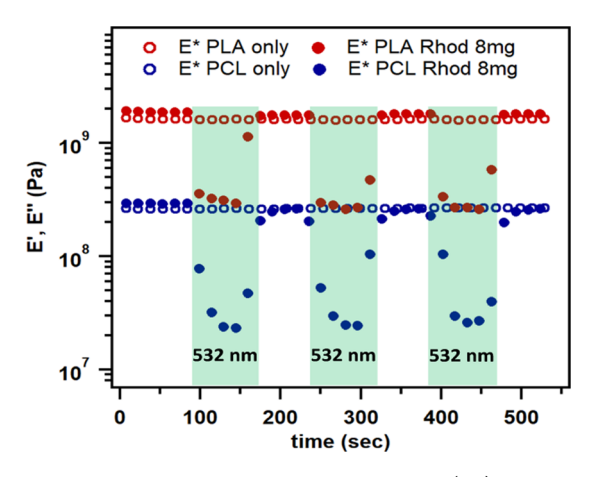


**Figure 7.** Reversible changes in complex modulus  $(E^*)$  of PLA mats (solid red circles) and PCL (solid blue circles) mats with 0.0191 mM rhodamine 6G after light irradiation 532 nm CW radiation (120 s, 100 mW cm<sup>-2</sup>). Radiation of PLA (empty red circles) and PCL (empty blue circles) with no dye added show no response to light stimulus.

the light irradiation (returns to slightly lower E' than the initial), but a complete recovery of modulus was observed for subsequent cycles. The DMA also shows that the PCL mats experienced a larger mechanical change during light irradiation than the corresponding PLA mats, which is consistent to the SEM images depicting the melting of the PCL mats. The PCL mats also show a slower response to the light stimulus in agreement to the angular displacement experiment. Namely, it takes  $\sim 4-5$  times longer for the PCL mats to reach a plateau in the complex modulus  $E^*$  value upon light radiation than for the PLA mats (Figure 7). Irradiation of both plain PCL and PLA polymer mats with no rhodamine 6G dye dispersed did not lead to any observable softening.

With the DMA quantification of the modulus change under a given light fluence, it is possible to compare the thermal bending model to other nonmuscular mechanical systems. Unfortunately, there is no current consensus on a benchmark figure of merit for photobending materials, so herein we propose two different approaches. The first analysis is taken from Skotheim and Mahadevan, who analyzed a large set of nonmuscular motions occurring in plants and fungi by relating the duration of the bending event to the dimension of the moving portion of the organism. The analysis reveals both an inertial time constant as well as the velocity of the elastic wave generated in the plant material. The analysis by Skotheim and Mahadevan yields a theoretical upper limit for both inertial response and velocity of the elastic wave to give an idea if

further optimization is possible in the material. It seems most appropriate to compare the motions of photomechanical materials to motions of plants since both classes of motions are nonmuscular. The second analysis is a calculation of work generated per photon fluence and represents an efficiency benchmark for current materials that undergo nonmuscular motion and displacement. Equations 1, 2, and 3 are for the calculation of the physical limit of an initial elastic wave  $(\tau_i)$ , velocity of the elastic wave, and work as a function of photon fluence, respectively. Equation 1 is for the calculation of the physical limit for initial elastic wave  $(\tau_i)$  where  $\rho$  is the bulk density, E is the modulus, and L is the thickness describing the medium containing the elastic wave. For our experiments, we estimate this as 0.4  $\mu$ m, which is determined from an average diameter of electrospun fibers extracted from a selection of SEM images (note that the energy travels down the backbone to the fiber).40 The modulus is known precisely from the DMA measurements.

$$\tau_{\rm i} = L \times \sqrt{\left(\frac{\rho}{E}\right)} \tag{1}$$

Equation 2 is for the upper limit for the velocity (m s<sup>-1</sup>) of the elastic wave, where  $\rho$  is the bulk density and E is the modulus.

velocity = 
$$\sqrt{\left(\frac{E}{\rho}\right)}$$
 (2)

Equation 3 is a measure of modulus efficiency and describes the amount of work performed by the change in modulus as a function of photon fluence, where  $\Delta E$  is the change in modulus, *l* is the optical penetration depth, *I* is the intensity (W m<sup>-2</sup>), and s is seconds. We have considered measuring the efficiency as the amount of observed deformation divided by input energy. Unfortunately, in many of our electospun mats, the deformation is limited to 90° because of the instrumentation and not inherent properties of the mats. Again, the change in modulus is determined directly from the DMA experiments, and the intensity and irradiation times are known. The optical penetration depth establishes the bilayer critical for bending. We estimate this from examination of the polymer mats videos under irradiation conditions and simply note the depth of observed dye emission radiating form the mat into the charge-coupled device camera. We used the thickness of a fiber as an internal ruler to approximate the optical penetration depth. Moreover, as stated above, we note that there is no observed transmission of light through the electrospun polymer mat. This efficiency term is unitless and represents the amount of work performed per energy input.

Table 1. Comparison of Benchmark Parameters for a Series of Materials

material	L (μm)	E (Pa)	$\Delta E$ (Pa)	l (m)	$\tau_{i}$ (s)	velocity	efficiency
PCL/0.0191 mM rhodamine	0.374 <sup>a</sup>	$4 \times 10^8$	$3.8 \times 10^{8}$	88 × 10 <sup>-6</sup> b	$6.3 \times 10^{-10}$	$5.9 \times 10^{5}$	0.37
PLA/0.0191 mM rhodamine	$0.4^a$	$3 \times 10^{9}$	$7.4 \times 10^{8}$	$88 \times 10^{-6}  ^{b}$	$2.6 \times 10^{-10}$	$2.6 \times 10^6$	0.72
RuSO/NB 1:40°	2.	$5 \times 10^{8}$	$2.1 \times 10^{8}$	$2 \times 10^{-6}$	$2.8 \times 10^{-9}$	$7.2 \times 10^{5}$	0.010
azo-LCN <sup>d</sup>	10	$1 \times 10^9$	$2.2 \times 10^{5}$	$2 \times 10^{-5}$	$9-11 \times 10^{-9}$	$1 \times 10^{6}$	0.16
diarylethene co-crystal <sup>e</sup>	30	$1.1 \times 10^{10}$	$44 \times 10^{6}$	$3 \times 10^{-5}$	$1 \times 10^{-8}$	$2.5 \times 10^{6}$	0.88
Venus flytrap <sup>f</sup>	500	$0.1 \times 10^{8}$		$1 \times 10^{-4}$	$5 \times 10^{-4}$	~105	

<sup>&</sup>lt;sup>a</sup>Average diameter of single fibers taken form SEM images. <sup>b</sup>Estimated effective "hot" bilayer thickness taken from emission of dye in polymer mat. <sup>c</sup>Mechanical parameters of polynorbornene-doped isomerizing ruthenium sulfoxide taken from Jin et al. <sup>31,33</sup> <sup>d</sup>Mechanical parameters of azobenzene containing liquid crystal networks at 50 °C taken from Yu et al. <sup>12,42</sup> <sup>e</sup>Mechanical parameters of diarylethene co-crystal taken from Morimoto and Irie. <sup>17</sup> <sup>f</sup>Mechanical parameters of the Venus flytrap taken form Mahadevan et al. <sup>5</sup>

This number can be greater than 1, but this value primarily reflects the  $\Delta E$  exhibited by the material following irradiation and includes release of strain formed during the fabrication of the material. For the electrospun mats described here, one expects this contribution to  $\Delta E$  to relatively large when compared to a thin film. For materials that show very little plastic deformation following irradiation, one may expect efficiency values less than unity. For example, for the PLA and PCL electrospun polymer mats described here, there is very little plastic deformation (<10%) as evidenced by the return to nearly identical modulus even after many irradiationrelaxation cycles (Figure 7). However, materials that feature large deformations due to changes in modulus may exhibit rather large efficiency values. We expect that many photosalient crystals will exhibit large efficiencies, as the  $\Delta E$  values expected from mechanical rupture (and failure) should be quite large.

$$efficiency = \frac{\Delta E \times l}{I \times s}$$
(3)

Shown in Table 1 are relevant data and benchmark quantities for a series of materials available in the literature and the materials presented in this work. The trend in the physical limit of the inertial time associate to the elastic wave shows that soft polymer materials are faster than the crystalline and biological materials. For the photoactive materials described in Table 1, these time constants are on the order of hundreds of picoseconds to nanoseconds (Venus flytrap is much slower and not phototriggered), and this response is likely a direct consequence of the exothermic processes associated to excited state decay of the chromophore in the material. Recalling eq 1,  $\tau_i$  is a primarily dependent upon the optical penetration depth. Note that neither E nor  $\rho$  of the polymer is affected or perturbed by the concentration of the dye in the polymer. This realization explains why the velocity of the elastic wave is relatively unchanged in these materials, since the velocity is dependent upon intrinsic properties of the material and as such any elastic wave (thermal, acoustic) will travel with the same speed through the material regardless of how the wave is initiated.

Although the range in efficiency for these materials is relatively modest, it may very well be borne out that much larger changes in efficiency will be observed once a larger set of samples can be compared. As noted above, this particular approach for measuring efficiency relies heavily upon the change in modulus, and the fact remains that all of these molecular materials are relatively soft. The inclusion of a wider array of materials will help provide context to this measure of efficiency in photonastic materials.

# CONCLUSIONS

We have demonstrated that electrospun nanofibrous polymer mats that contain simple, nonisomerizing dyes when irradiated generate rapid macroscale movements. We have found that a photothermal mechanism is operative, where the time required for bending and extent of bending are determined by dye loading, light exposure, and nanofiber structure. The heat that is absorbed by the dye and then subsequently released through nonradiative decay leads to a change in the elastic modulus of the material. Moreover, we suspect that this photothermal heating also releases strain that is introduced during the electrospinning preparation of these nanofibrous mats. Future

studies will continue to investigate this photothermal bending mechanism in these materials.

## **ASSOCIATED CONTENT**

## S Supporting Information

The Supporting Information is available free of charge on the ACS Publications website at DOI: 10.1021/acsami.8b11294.

> All home built and commercial instrumentation; analytical methods; electronic absorbance; emission and reflectance spectra of the dyes in solution and polymer mats; angular displacement vs time and power for all rhodamine 6G PCL and PLA mats; velocity vs time for all rhodamine 6G PCL and PLA mats; acceleration vs time for all rhodamine 6G PCL and PLA mats; angular displacement velocity and acceleration for select H2TPP PCL and PLA mats; in-depth modulus changes for rhodamine 6G and H2TPP PLA mats; SEM of pure PLA mat (PDF)

> Rhodamine 6G in PLA mat bending and PLA film morphology control (AVI)

Plain PLA mat bending using a nichrome wire (AVI) PLA mat reversible bending multiple times (AVI)

#### AUTHOR INFORMATION

## **Corresponding Authors**

\*E-mail: alexiso@bgsu.edu (A.D.O.). \*E-mail: jrack@unm.edu (J.J.R.).

## ORCID ®

Yang Qin: 0000-0002-5764-8137

Alexis D. Ostrowski: 0000-0002-3207-1845 Jeffrey J. Rack: 0000-0001-6121-879X

#### **Notes**

The authors declare no competing financial interest.

# ACKNOWLEDGMENTS

J.J.R. acknowledges NSF (Grant CHE 1602240) and the University of New Mexico for financial support. A.D.O. acknowledges the NSF CAREER award (CHE-1653892) and Bowling Green State University for financial support.

#### REFERENCES

- (1) Raven, J. A. The Cost of Photoinhibition. Physiol. Plant. 2011, 142, 87-104.
- (2) Christie, J. M.; Murphy Angus, S. Shoot Phototropism in Higher Plants: New Light Through Old Concepts. Am. J. Bot. 2013, 100, 35-
- (3) Iino, M. Phototropism Mechanisms and Ecological Implications. Plant, Cell Environ. 1990, 13, 633-650.
- (4) Koller, D. Plants in Search of Sunlight. In Advances in Botanical Research; Academic Press, 2000; pp 35-131.
- (5) Skotheim, J. M.; Mahadevan, L. Physical Limits and Design Principles for Plant and Fungal Movements. Science 2005, 308, 1308-
- (6) Forterre, Y.; Skotheim, J. M.; Dumais, J.; Mahadevan, L. How the Venus Flytrap Snaps. Nature 2005, 433, 421-425.
- (7) Foster, K. W.; Saranak, J.; Patel, N.; Zarilli, G.; Okabe, M.; Kline, T.; Nakanishi, K. A Rhodopsin is the Functional Photoreceptor for Phototaxis in the Unicellular Eukaryote Chlamydomonas. Nature 1984, 311, 756-759.
- (8) Koerner, H.; White, T. J.; Tabiryan, N. V.; Bunning, T. J.; Vaia, R. A. Photogenerating Work from Polymers. Mater. Today 2008, 11, 34-42.

- (9) Yu, H.; Ikeda, T. Photocontrollable Liquid-Crystalline Actuators. *Adv. Mater.* **2011**, 23, 2149–2180.
- (10) Commins, P.; Desta, I. T.; Karothu, D. P.; Panda, M. K.; Naumov, P. Crystals on the Move: Mechanical Effects in Dynamic Solids. *Chem. Commun.* **2016**, *52*, 13941–13954.
- (11) Abendroth, J. M.; Bushuyev, O. S.; Weiss, P. S.; Barrett, C. J. Controlling Motion at the Nanoscale: Rise of the Molecular Machines. *ACS Nano* **2015**, *9*, 7746–7768.
- (12) Yu, Y.; Nakano, M.; Ikeda, T. Photomechanics: Directed Bending of a Polymer Film by Light. *Nature* **2003**, *425*, 145.
- (13) Harris, K. D.; Cuypers, R.; Scheibe, P.; van Oosten, C. L.; Bastiaansen, C. W. M.; Lub, J.; Broer, D. J. Large Amplitude Light-Induced Motion in High Elastic Modulus Polymer Actuators. *J. Mater. Chem.* **2005**, *15*, 5043–5048.
- (14) Agrawal, A.; Yun, T. H.; Pesek, S. L.; Chapman, W. G.; Verduzco, R. Shape-Responsive Liquid Crystal Elastomer Bilayers. *Soft Matter* **2014**, *10*, 1411–1415.
- (15) Tong, F.; Liu, M.; Al-Kaysi, R. O.; Bardeen, C. J. Surfactant-Enhanced Photoisomerization and Photomechanical Response in Molecular Crystal Nanowires. *Langmuir* **2018**, *34*, 1627–1634.
- (16) Al-Kaysi, R. O.; Tong, F.; Al-Haidar, M.; Zhu, L.; Bardeen, C. J. Highly branched photomechanical crystals. *Chem. Commun.* **2017**, *53*, 2622–2625.
- (17) Morimoto, M.; Irie, M. A Diarylethene Cocrystal that Converts Light into Mechanical Work. *J. Am. Chem. Soc.* **2010**, *132*, 14172–14178.
- (18) Naumov, P.; Chizhik, S.; Panda, M. K.; Nath, N. K.; Boldyreva, E. Mechanically Responsive Molecular Crystals. *Chem. Rev.* **2015**, 115, 12440–12490.
- (19) Kitagawa, D.; Tsujioka, H.; Tong, F.; Dong, X.; Bardeen, C. J.; Kobatake, S. Control of Photomechanical Crystal Twisting by Illumination Direction. *J. Am. Chem. Soc.* **2018**, *140*, 4208–4212.
- (20) Koshima, H.; Ojima, N.; Uchimoto, H. Mechanical Motion of Azobenzene Crystals upon Photoirradiation. *J. Am. Chem. Soc.* **2009**, 131, 6890–6891.
- (21) Koshima, H.; Takechi, K.; Uchimoto, H.; Shiro, M.; Hashizume, D. Photomechanical Bending of Salicylideneaniline Crystals. *Chem. Commun.* **2011**, *47*, 11423–11425.
- (22) Bushuyev, O. S.; Tomberg, A.; Friščić, T.; Barrett, C. J. Shaping Crystals with Light: Crystal-to-Crystal Isomerization and Photomechanical Effect in Fluorinated Azobenzenes. *J. Am. Chem. Soc.* **2013**, *135*, 12556–12559.
- (23) Wang, H.; Chen, P.; Wu, Z.; Zhao, J.; Sun, J.; Lu, R. Bending, Curling, Rolling, and Salient Behavior of Molecular Crystals Driven by [2 + 2] Cycloaddition of a Styrylbenzoxazole Derivative. *Angew. Chem., Int. Ed.* **2017**, *56*, 9463–9467.
- (24) Nath, N. K.; Runčevski, T.; Lai, C.-Y.; Chiesa, M.; Dinnebier, R. E.; Naumov, P. Surface and Bulk Effects in Photochemical Reactions and Photomechanical Effects in Dynamic Molecular Crystals. J. Am. Chem. Soc. 2015, 137, 13866–13875.
- (25) Medishetty, R.; Sahoo, S. C.; Mulijanto, C. E.; Naumov, P.; Vittal, J. J. Photosalient Behavior of Photoreactive Crystals. *Chem. Mater.* **2015**, *27*, 1821–1829.
- (26) Liu, Y.; Gall, K.; Dunn, M. L.; Greenberg, A. R.; Diani, J. Thermomechanics of Shape Memory Polymers: Uniaxial Experiments and Constitutive Modeling. *Int. J. Plast.* **2006**, 22, 279–313.
- (27) Lendlein, A.; Kelch, S. Shape-Memory Polymers. *Angew. Chem., Int. Ed.* **2002**, *41*, 2034–2057.
- (28) Wereley, N. M.; Sater, J. M. Plants and Mechanical Motion: A Synthetic Approach to Nastic Materials and Structures; DEStech Publications, 2012.
- (29) Agolini, F.; Gay, F. P. Synthesis and Properties of Azoaromatic Polymers. *Macromolecules* **1970**, *3*, 349–351.
- (30) Razgoniaev, A. O.; Butaeva, E. V.; Iretskii, A. V.; Ostrowski, A. D. Changing Mechanical Strength in Cr(III)- Metallosupramolecular Polymers with Ligand Groups and Light Irradiation. *Inorg. Chem.* **2016**, *55*, 5430–5437.

- (31) Jin, Y.; Harrington, D.; Rachford, A. A.; Rack, J. J. Stimulating Changes in the Elastic Modulus of Polymer Materials by Molecular Photochromism. *RSC Adv.* **2014**, *4*, 62920–62925.
- (32) Jin, Y.; Rack, J. J. Molecules in Motion: From Sub-Nanoscale to Macroscale. *Isr. J. Chem.* **2013**, *53*, 280–287.
- (33) Jin, Y.; Paris, S. I. M.; Rack, J. J. Bending Materials with Light: Photoreversible Macroscopic Deformations in a Disordered Polymer. *Adv. Mater.* **2011**, 23, 4312–4317.
- (34) Razgoniaev, A. O.; Mikhailov Kirill, I.; Obrezkov Filipp, A.; Butaeva Evgeniia, V.; Ostrowski Alexis, D. Supramolecular Elastomers: Switchable Mechanical Properties and Tuning Photohealing with Changes in Supramolecular Interactions. *J. Polym. Sci., Part A: Polym. Chem.* **2018**, *56*, 1003–1011.
- (35) Aono, M.; Harata, T.; Kitazawa, N.; Watanabe, Y. Reversible photo-induced deformation of amorphous carbon nitride thin films. *Diamond Relat. Mater.* **2014**, *41*, 20–24.
- (36) Adler, A. D.; Longo, F. R.; Finarelli, J. D.; Goldmacher, J.; Assour, J.; Korsakoff, L. A simplified synthesis for mesotetraphenylporphine. *J. Org. Chem.* **1967**, *32*, 476.
- (37) Montalti, M.; Credi, A.; Prodi, L.; Gandolfi, M. T. Handbook of Photochemistry, 3rd ed.; CRC Press, 2006.
- (38) Schneider, C. A.; Rasband, W. S.; Eliceiri, K. W. NIH Image to ImageI: 25 Years of Image Analysis. *Nat. Methods* **2012**, *9*, 671–676.
- (39) Wypych, G. Handbook of Polymers; ChemTec Publishing, 2012.
- (40) Uetani, K.; Okada, T.; Oyama, H. T. Crystallite Size Effect on Thermal Conductive Properties of Nonwoven Nanocellulose Sheets. *Biomacromolecules* **2015**, *16*, 2220–2227.
- (41) Uetani, K.; Ata, S.; Tomonoh, S.; Yamada, T.; Yumura, M.; Hata, K. Elastomeric Thermal Interface Materials with High Through-Plane Thermal Conductivity from Carbon Fiber Fillers Vertically Aligned by Electrostatic Flocking. *Adv. Mater.* **2014**, *26*, 5857–5862.
- (42) Yu, Y.; Maeda, T.; Mamiya, J.; Ikeda, T. Photomechanical Effects of Ferroelectric Liquid-Crystalline Elastomers Containing Azobenzene Chromophores. *Angew. Chem., Int. Ed.* **2007**, *46*, 881–883.